Journal of Nuclear Materials 400 (2010) 119–126

Contents lists available at ScienceDirect

Journal of Nuclear Materials

journal homepage: www.elsevier.com/locate/jnucmat

Phase equilibria in the FeO_{1+x}–UO_2–ZrO_2 system in the FeO_{1+x}-enriched domain

V.I. Almjashev [a], M. Barrachin [b], S.V. Bechta [c], D. Bottomley [d], F. Defoort [e], M. Fischer [f], V.V. Gusarov [g], S. Hellmann [f], V.B. Khabensky [c], E.V. Krushinov [c], D.B. Lopukh [a], L.P. Mezentseva [h,*], A. Miassoedov [i], Yu.B. Petrov [a,1], S.A. Vitol [c]

[a] Saint Petersburg Electrotechnical University 'LETI', Prof. Popov str., 5, St. Petersburg 197376, Russian Federation
[b] Institut de Radioprotection et Sûreté Nucléaire (IRSN), BP 3 F-13115 St-Paul-Lez-Durance, France
[c] A.P. Aleksandrov Research Institute of Technology, NITI, DSAR, Sosnovy Bor 188540, Russian Federation
[d] EC, Joint Research Centre, Institute for Transuranium Elements, Postfach 2340, Hermann-von-Helmholtz-Pl. 1, 76125 Karlsruhe, Germany
[e] Laboratoire de Physico-chimie et Thermohydraulique Multiphasiques (LPTM), CEA/Grenoble, DTN/SE2T/LPTM, 17 Rue des Martyrs, 38 054 Grenoble cedex 9, France
[f] AREVA NP GmbH, Freyeslebenstr. 1, 91058 Erlangen, Germany
[g] Saint Petersburg State Institute of Technology (Technical University), Moskovsky Av., 26, St. Petersburg 190013, Russian Federation
[h] Institute of Silicate Chemistry of Russian Academy of Sciences, Makarov Emb., 2, St. Petersburg 199034, Russian Federation
[i] Karlsruhe Institute of Technology, Campus North, Hermann-von-Helmholtz-Platz 1, 76344 Eggenstein-Leopoldshafen, Germany

ARTICLE INFO

Article history:
Received 5 June 2008
Accepted 23 February 2010

ABSTRACT

Experimental results of the investigation of the FeO_{1+x}–UO_2–ZrO_2 system in neutral atmosphere are presented. The ternary eutectic position and the composition of the phases crystallized at this point have been determined. The phase diagram is constructed for the FeO_{1+x}-enriched region and the onset melting temperature of 1310 °C probably represents a local minimum and so will be a determining factor in this system and its application to safety studies in nuclear reactors.

1. Introduction

During the analysis of postulated severe accidents with core melting in nuclear power plants (NPP) one of the key issues is a reliable prediction of the physicochemical behavior of molten materials containing fuel, cladding and steel. Typically, during in-vessel scenarios, such melts result from the interaction between the UO_2 fuel, Zircaloy or Zr cladding and internal steel structures. Moreover, in the course of the accident the molten material is subjected to steam oxidation and interaction with the surrounding steel of the pressure vessel as it was considered, for example, by Tuomisto and Theofanous [1] and Bechta et al. [2]. Therefore, the information on phase equilibria in the FeO_{1+x}–UO_2–ZrO_2 system, melting and crystallization temperatures, i.e. the positions of the solidus and liquidus surfaces in this system, are very important for the analysis of molten pool behavior and its interaction with the reactor vessel steel.

The data available in the literature for this system are quite limited. Recently the corium interaction thermochemistry (CIT) project (from the 4th FP of the European Commission) examined some key coria compositions relating to European Pressure Reactor (EPR)-type melt. A liquidus temperature of 1946 ± 20 °C was measured for the 55.0 FeO_{1+x}–23.6 UO_2–21.4 ZrO_2 (mol.%) composition (corium named CIT-R in [2,P.1362]). Nevertheless, it was only a single measurement that provides a first indication of the behavior of the FeO_{1+x}–UO_2–ZrO_2 system (among other relevant phase systems). In fact, only phase diagrams of the corresponding binary systems have been experimentally investigated, while the phase diagram of the ternary oxide system has not even been experimentally constructed except for the liquidus temperature measurements by the authors in previous works Bechta et al. [2] and Adroguer [3].

The UO_2–FeO_{1+x} system was studied by Lopukh et al. [4] in a narrow concentration region of the FeO_{1+x}-rich system, where the position of the eutectic point was determined as 1340 °C and 3.3 mol.% UO_2. The publications of Bechta et al. [5,6] have presented a more complete version of the phase diagram of the UO_2–FeO_{1+x} system in which the eutectic point (1335 ± 5 °C, 4.0 ± 0.1 mol.% UO_2) slightly differs from the data in [4]. This seems to arise from differences between the FeO_{1+x} stoichiometry in this work, because the onset melt temperature of the FeO_{1+x}-based phase and the liquidus line position is known to change with the Fe:O ratio according to Darken and Gurry' phase diagram [7]. The results presented by Bechta et al. [6] confirm this conclusion.

The ZrO_2–FeO_{1+x} system was investigated in [8–10]. In Fischer and Hoffmann [8] the study was carried out in the 1300–1800 °C temperature range. The phase diagram of the ZrO_2–FeO_{1+x} system in a wider temperature range is presented by Bechta et al. [9,10]. The results given in [8] and [9,10] have significant differences in

* Corresponding author. Address: ul. Karbysheva, d. 10, kv. 108, Saint-Petersburg, 194021, Russian Federation. Tel.: +7 812 325 41 36; fax: +7 812 328 85 89.
E-mail address: la_mez@mail.ru (L.P. Mezentseva).
[1] Deceased.

0022-3115/$ - see front matter © 2010 Elsevier B.V. All rights reserved.
doi:10.1016/j.jnucmat.2010.02.020

(1) the positions of solidus and liquidus lines, (2) the data on the solid solution decomposition in the subsolidus region and (3) the transition temperatures. As shown by Bechta et al. [10], the divergence of the data on the ZrO_2–FeO_{1+x} phase diagram of these publications is associated with differences in experimental techniques and in data interpretation.

Phase equilibria of the UO_2–ZrO_2 system were studied by Lambertson and Mueller [11], Wollten [12], Evans [13], Voronov et al. [14,15], Cohen and Schaner [16], Baes et al. [17], Bottomley and Coquerelle [18] and Skokan [19]. It should be noted that there were significant differences in the phase diagrams constructed by various authors. These differences are related to both solidus and liquidus lines and phase compositions of the system in the subsolidus region. While in Evans [13] the UO_2–ZrO_2 system is presented as a eutectic type diagram with limited solid solutions, in all other studies these diagrams have a minimum in the liquidus and solidus curves. Much attention was paid to the investigation of the UO_2–ZrO_2 subsolidus region by Evans [13], Cohen and Schaner [16] and Baes et al. [17]. In [16], the system was studied in detail in the temperature range from 1200 °C up to the tetragonal-cubic transition temperature of ZrO_2. In the work [17] the solubility limits of UO_2 in ZrO_2 and ZrO_2 in UO_2 were determined for the tetragonal solid solutions just below the tetragonal-monoclinic transition temperature of ZrO_2, i.e. near 1100 °C. It should be noted that the solid solution limits determined by the extrapolation of the experimental results of [13] and [16] down to the lower temperature region and from the data of [17] up to a high temperature region have a significant divergence. The disparity on the mutual solubility of the components is particularly noticeable in solid state in the temperature range below 1500 °C [16,17].

From the modeling point of view, the FeO_{1+x}–UO_2–ZrO_2 pseudo-ternary phase diagram calculation is available within the frameworks of the NUCLEA European Thermodynamic Database for Corium Applications by Cheynet [20]. It is based, in the absence of experimental data, on the CALPHAD optimization of the three pseudo-binary sections UO_2–ZrO_2, FeO_{1+x}–UO_2 and FeO_{1+x}–ZrO_2. For the UO_2–ZrO_2 phase diagram, the details of the optimization were reported in Chevalier et al. [21]. They in particular selected the measurements of Lambertson and Mueller [11] at high temperature which exhibit a minimum in the liquidus and solidus curves and a very low ZrO_2 solubility in UO_2 at a low temperature (<1500 °C) in accordance with the experimental data of Romberger et al. [22]. For the UO_2–FeO_{1+x} and ZrO_2–FeO_{1+x} systems, the modeling recently proposed in Bakardjieva et al. [23] reproduces the topologies as experimentally determined in Bechta et al. [6,10]. With this "rather" simplified approach, i.e. only derived from the optimization of the binary systems, the calculated liquidus temperature for the composition of the corium named CIT-R (previously mentioned) 55.0 $Fe_{0.947}O$ –23.6 UO_2–21.4 ZrO_2 (mol.%), is predicted to be 1910 °C, i.e. in good agreement with the experimental determination (1946 ± 20 °C). Nevertheless, the available experimental data are too scarce for a validation of the approach.

Given the FeO_{1+x}-rich eutectic of the UO_2–FeO_{1+x} (Fig. 1a) and ZrO_2–FeO_{1+x} (Fig. 1b) phase diagrams, combined with the limited mutual solubility of the UO_2–ZrO_2 system (Fig. 1c) at the eutectic temperatures of the UO_2–FeO_{1+x} (1335 ± 5 °C) and ZrO_2–FeO_{1+x} systems (1332 ± 5 °C), as well as the high-temperature solidus in the UO_2–ZrO_2 system would imply that the ternary eutectic point is located in the FeO_{1+x}-enriched region of the FeO_{1+x}–UO_2–ZrO_2 system. The ternary eutectic is also likely to have the lowest

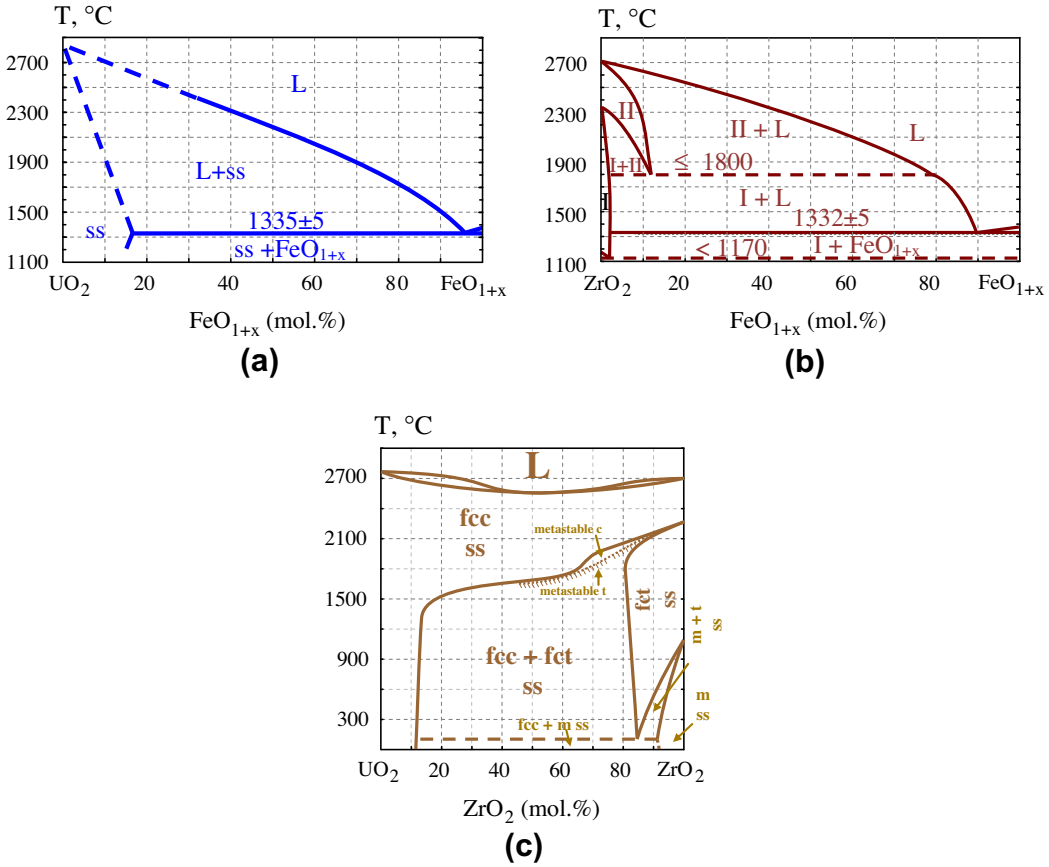

Fig. 1. Phase diagrams of the systems: (a) UO_2–FeO_{1+x} (inert atmosphere) by Bechta et al. [6], ss – urania-based solid solutions; (b) ZrO_2–FeO_{1+x} (inert atmosphere) by Bechta et al. [10], (I) – *t*-ZrO_2(FeO)-based solid solutions, (II) – *c*-ZrO_2(FeO)-based solid solutions; (c) UO_2–ZrO_2 by Cohen [16], fcc ss – face-centered cubic solid solutions, fct ss – face-centered tetragonal solid solutions, m ss – monoclinic solid solutions.

temperature, at which a liquid phase appears in the FeO_{1+x}–UO_2–ZrO_2 system. Thus the objectives of this article are to investigate the FeO_{1+x} region of the ternary phase diagram and then to determine this lowest temperature and eutectic composition in neutral atmosphere above the melt.

2. Materials and methods

The initial substances for the specimen preparation were as follows: ZrO_2 (>99.3 mass% purity), pure UO_2 (>99.0 mass% purity, Fe, As, CuO, phosphates, chlorides not more than 0.07 mass%), FeO_{1+x} (not less than 99.0 mass%, impurities insoluble in HCl, sulphates, chlorides not more than 0.8 mass%) and pure Fe (>99.9 mass% purity).

Initial components were mixed and melted in the "Rasplav 2" and "Rasplav 3" facilities by Induction Melting in a Cold Crucible (IMCC) under flowing argon Petrov [24]. When the melt was homogeneous, it was slowly cooled down until completely solidified.

In order to crystallize iron oxide as a wüstite structure (FeO_{1+x}) with a composition closest to the FeO stoichiometry given by the phase diagram in [7], metallic iron was admixed as a getter in the quantity of 1 mass% of the total mass. The ingots were then sectioned and smaller samples taken from the various regions as determined by visual inspection. These samples were then mounted and polished for further microscopic analysis. The microstructure of the specimen, its elemental composition and the composition of the phases were analyzed by scanning electron microscopy (SEM) and energy-dispersive X-ray spectrometry (EDX) using the ABT-55 coupled with the Oxford Link microprobe analyzer. The error in determining the elemental content by this method varies with the atomic number and equals to ±0.3 mass% on average. In the present work the content of oxygen in the solid phases was not determined directly. Conclusions were based both on the cation ratio and the XRD phase analysis.

About 7 mg specimens were cut out from the eutectic zone of the ingot bulk as observed by electron microscopy observations and were investigated by visual polythermal analysis (VPA) in the Galakhov microfurnace [25] and by differential thermal analysis (DTA). The melting temperature was determined by VPA in the Galakhov microfurnace using the technique described in Bechta et al. [9] with an experimental error not exceeding 30 °C in Bechta et al. [9,10] and Almjashev et al. [26]. Thermal transformations in the system were studied by DTA using the SETARAM SETSYS Evolution-2400 apparatus. The temperatures of the thermal effects were determined from the corresponding peak onset in the DTA curves. The peak onset was identified by the intersection in the tangents extrapolated from the baseline and the thermal effect curve. The heating rate was 5 °C/min and the atmosphere was neutral (high purity helium). The error of the temperature determination by this device was ±5 °C expected with the standard procedure of calibration. As the Al_2O_3 crucible intensively interacted with the specimen after a liquid phase occurrence observed in Bechta et al. [6], only phase transition temperatures in the subsolidus region and solidus temperature (eutectic temperature in particular; see Bechta et al. [6,10]) could be measured with adequate reliability.

Another sample, which was also cut out from the eutectic zone of the ingot was studied by XRD using the DRON-3 X-ray diffractometer with the Co K_α-radiation (λ = 178.897 pm) in order to confirm or refute wüstite phase in the eutectic composition.

3. Discussion of results

Crystallization of the melt was carried out from the regions of primary crystallization of the U and Fe oxide-based phases to determine the eutectic point in the FeO_{1+x}–UO_2–ZrO_2 system. For the UO_2–FeO_{1+x} (Fig. 1a) system, a good agreement with experimental data in respect of the liquidus curve is given by the simple model of ideal solutions in Bechta et al. [6]. By contrast calculations with the model of ideal solutions for the ZrO_2–FeO_{1+x} system (Fig. 1b) are not in satisfactory agreement with the experimental data. The use of a model of regular solutions has not given satisfactory results either. Therefore the ternary eutectic position has been estimated as a geometrical optimum derived from the experimentally determined coordinates of the binary eutectics of the ZrO_2–FeO_{1+x} and the UO_2–FeO_{1+x} systems.

Based on the calculations of the primary UO_2 crystallization region, a melt of the following composition: 88.1 FeO_{1+x}–7.0 UO_2–4.9 ZrO_2 (mol.%) was produced by IMCC in the first test. Microstructure, phase content and chemical composition of the sample produced by slow melt crystallization are presented in Fig. 2 and in the Table 1. In all bulk regions of the specimen the microstructure typical for eutectic crystallization was found (Fig. 2). The chemical composition of the regions determined by EDX (Table 1) is practically the same, which confirms their large-scale homogeneity.

The elemental analysis of the phases coexisting in the eutectically crystallized regions exhibiting an eutectic-type morphologies showed that UO_2- and ZrO_2-based phases are the solid solutions while UO_2 and ZrO_2 are practically not dissolved in FeO_{1+x} (Table 1, analyses of zones 1 and 2). It should be noticed that the content of FeO_{1+x} and UO_2 determined by SEM/EDX could be significantly overestimated due to a very small size of grains of the ZrO_2 solid solution (Fig. 2).

In the second test, a melt of 96.0 FeO_{1+x}–2.0 UO_2–2.0 ZrO_2 (mol.%) composition located in the primary FeO_{1+x} crystallization region was prepared by IMCC. The onset melting temperature of the sample was T_{sol} = 1315 °C according to VPA Galakhov microfurnace measurements. SEM/EDX data of the specimen are presented in Fig. 3 and in the Table 1. The microstructure of the central regions is homogeneous (Fig. 3) and their chemical composition (Table 1, SQ1–2 for Fig. 3) is very close to the eutectic composition given in the Table 1 for Fig. 2 (SQ1–6).

As it was noticed in the previous work Bechta et al. [5] the UO_2- and ZrO_2-based solid solutions (SS) decompose on cooling forming a thick FeO layer around SS grains (Figs. 2b,c and 3d) due to the FeO significant solubility decreasing along with temperature decreasing.

The XRD powder pattern (Fig. 4) obtained with an inner standard (Ge) allowed the estimation of the unit cell parameters of the cubic $(U,Zr)O_2$-based solid solution (a = 0.44255 ± 0.00005 nm), the tetragonal $(Zr,U)O_2$-based solid solution (a = 0.3642 ± 0.0002, c = 0.5208 ± 0.0002 nm) and the FeO_{1+x} phase (a = 0.43091 ± 0.00009 nm). The latter corresponds to $FeO_{1.059}$ in accordance with the linear dependence of a unit cell parameter for FeO_{1+x} phase with oxygen content as in Toropov et al. [27]. So, the final $Fe_{1-\delta}O$ (FeO_{1+x}) composition varies depending on the cooling rate of the sample and phase composition in the system (for the same p_{O_2} condition). Nevertheless, the value of the structural parameter indicates that it is within the region of wüstite existence in the Fe–O phase diagram by Wriedt [28].

The composition of the phases crystallized at the ternary eutectic point and the eutectic composition determined by EDX analysis from different fragments of the eutectic zone are given in Figs. 5 and 6. These data show that eutectic compositions determined at melt crystallization are close to each other, but a systematic shift of the compositions from the different areas of the phase diagram towards the domain of the primary crystallization phase is evident. Too fast cooling the melt (quenching) near the ternary eutectic point can result in the deviation from the equilibrium composition. Therefore, the most reliable and closest value to the real eutectic is the weighted average value, which is produced by statistical processing of the experimental data of SQ1–5 and SQ1–2 areas in

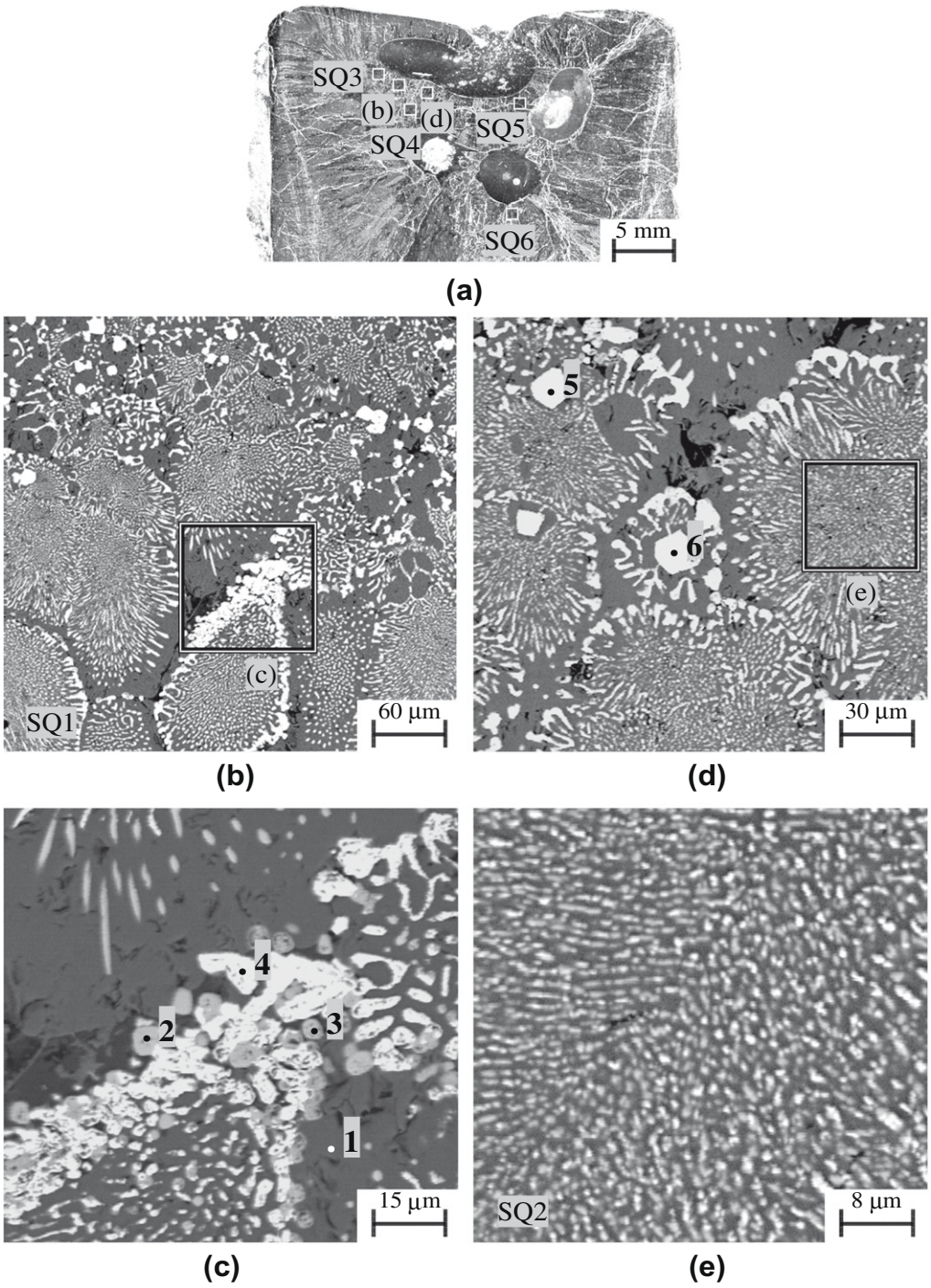

Fig. 2. General view (a) and micrographs (b–e) of the specimen produced by the melt crystallization in the eutectic crystallization region (UO_2 side): 88.1 FeO_{1+x}–7.0 UO_2–4.9 ZrO_2 (mol.%).

the Table 1 (see also Figs. 2 and 3 for the location). This is equal to 91.8 ± 0.5 FeO_{1+x}–3.8 ± 0.3 UO_2–4.4 ± 0.4 ZrO_2 (mol.%) and illustrated in the phase diagram as a central point of the oval eutectic region in Fig. 6.

The analysis of the UO_2-rich phases found in the two ingots, i.e. zones 5 and 6 of Fig. 2 in the Table 1 as well as zone 2 of Fig. 3 in the Table 1 gave a weighted average composition of 79.2 ± 1.2 UO_2–10.8 ± 1.9 ZrO_2–10.0 ± 1.6 FeO_{1+x} (mol.%). Zone 4 of Fig. 2 in the Table 1 shows the deviation from the real composition due to high dispersive crystallization and grains of ZrO_2-based solid solution presence near it. These are marked as small crosses at the top of the diagram in Fig. 5. They correspond satisfactorily to the data available from Bechta et al. [5,6], Evans [13], Voronov et al. [14,15] and Cohen and Schaner [16].

By contrast, the data obtained from the composition of the ZrO_2-based solid solution coexisting with the FeO_{1+x}- and UO_2-based phases at T = 1310–1315 °C considerably diverge from the expected results (that is, the small crosses in the lower half of the phase diagram in Fig. 5 lie above the dashed line). This may be due to errors of the EDX determination of the highly dispersed ZrO_2-based phase (Fig. 2c) because small volumes of adjacent phases also distort the result. Overlaps in the minor peaks of the

Table 1
EDX analysis of regions marked in Figs. 2 and 3.

Region, figure		FeO_{1+x} (mol.%)	UO_2 (mol.%)	ZrO_2 (mol.%)
SQ1, Fig. 2b		91.2	4.0	4.8
SQ2, Fig. 2e		91.5	3.6	4.9
SQ3, Fig. 2a		91.9	3.5	4.6
SQ4, Fig. 2a		91.7	4.0	4.3
SQ5, Fig. 2a		91.5	3.7	4.8
SQ6, Fig. 2a		91.4	4.2	4.4
1, Fig. 2c		100	–	–
2, Fig. 2c		20.2	21.5	58.3
3, Fig. 2c		22.0	19.9	58.1
4, Fig. 2c		6.6	74.6	18.8
5, Fig. 2d		8.3	78.8	12.9
6, Fig. 2d		11.6	78.4	10.0
SQ1, Fig. 3b		92.4	3.5	4.1
SQ2, Fig. 3c		92.7	3.6	3.7
1, Fig. 3d		100	–	–
2, Fig. 3d		10.1	80.6	9.3
Eutectic composition	Average value	91.8 ± 0.5	3.8 ± 0.3	4.4 ± 0.4
FeO_{1+x}-based phase		100	–	–
UO_2-based phase		10.0 ± 1.6	79.2 ± 1.2	10.8 ± 1.9

Note: oxygen content was not determined by EDX analysis (stoichiometric composition is calculated using the cations content determined by EDX).

U and Zr EDX analysis could also cause deviations. Therefore, this indicates the necessity of a more detailed study of phase equilibria in the low UO_2 concentration subsolidus domain of the UO_2–ZrO_2 system.

Comparing the compositions of the coexisting solid solutions observed here with the published data on the mutual solubility of the UO_2–FeO_{1+x}, ZrO_2–FeO_{1+x} and UO_2–ZrO_2 binary oxide systems (Fig. 5: different signs – published data; small crosses – this paper) shows that the results of [13–16] for the UO_2–ZrO_2 system in the 1310–1315 °C temperature range seem to be more consistent with the present results for the UO_2-enriched region than the data produced in the later Baes' study [17] by extrapolation up to higher temperatures. Therefore, the results of Evans [13], Voronov et al. [14,15] and Cohen and Schaner [16] were also chosen to predict the region of the ZrO_2-based solid solutions (Fig. 5, dashed lines).

For a more exact determination of the eutectic temperature, DTA was used in addition to VPA in the Galakhov microfurnace. Samples were cut out from the ingot bulk which had a eutectic crystallization character according to the SEM analysis. DTA thermograms of these samples are shown in Fig. 7 and yield a eutectic temperature of 1310 °C. The higher value of the eutectic temperature determined by the VPA Galakhov microfurnace could be caused by the systematic measurement errors of the method,

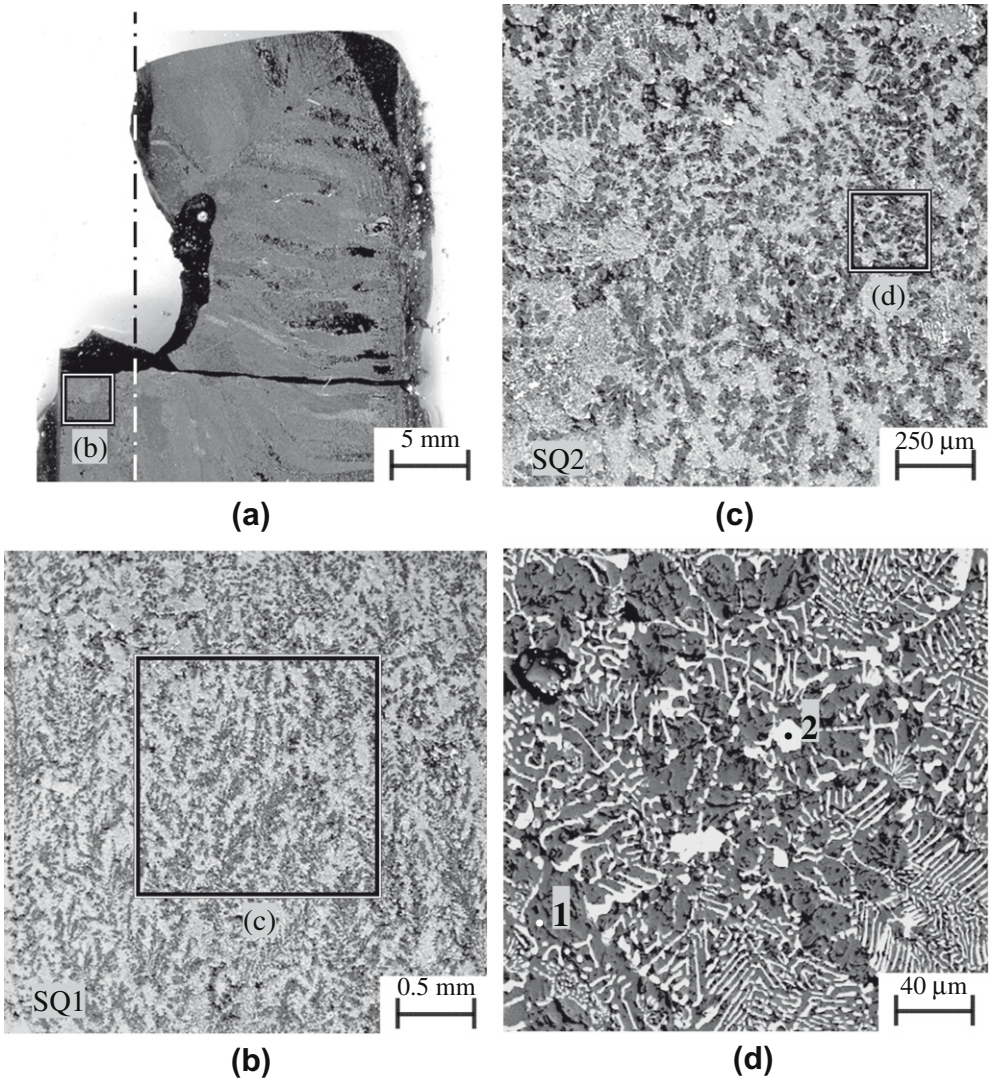

Fig. 3. General view (a) and micrographs (b–d) of the specimen produced by the melt crystallization in the eutectic crystallization region (FeO_{1+x} side): 96.0 FeO_{1+x}–2.0 UO_2–2.0 ZrO_2 (mol.%).

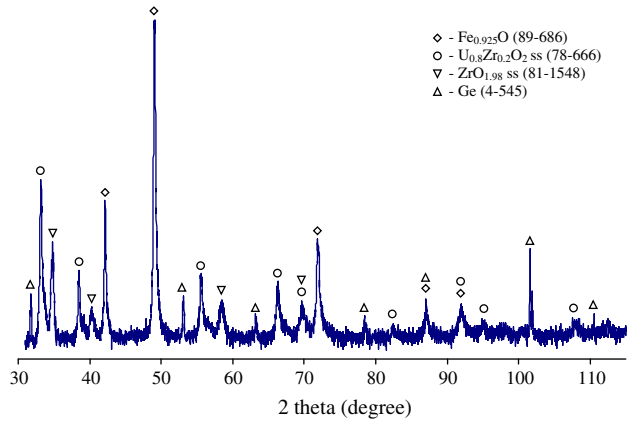

Fig. 4. X-ray diffraction pattern with inner Ge standard of the FeO_{1+x}–UO_2–ZrO_2 system specimen taken from the eutectic zone (Fig. 2, SQ5).

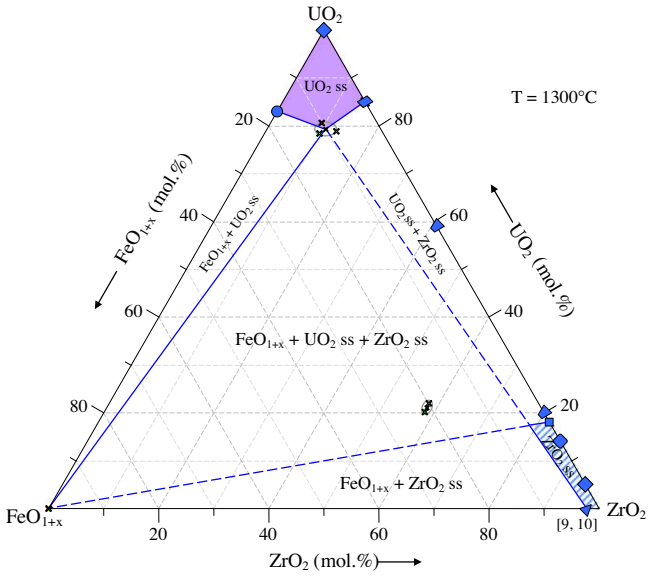

Fig. 5. The isothermal section of the FeO_{1+x}–UO_2–ZrO_2 system just below the ternary eutectic. The coexisting solid phases composition data from corresponding references: ● – [5,6]; ◥ – [9,10]; ◆ – [11,12]; ◆ – [13–16]; ■ – [13,16]; ◆ – [14,15]; ◆ – [17]; ✕ – present work according to SEM/EDX analysis; ⬭ – the region of the mean square deviation of the experimental data; ▭ – solid solutions region (experiment); ▨ – solid solution (modeling); — – tie-line (modeling); — — – tie-line (based on literature).

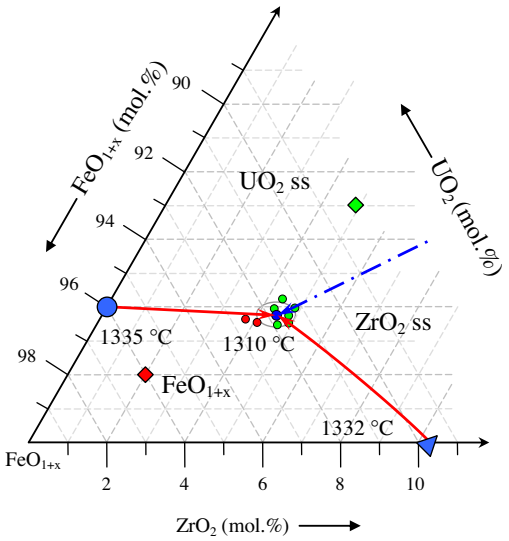

Fig. 6. Fusion diagram (FeO_{1+x}-enriched region) (neutral atmosphere). ◆,▲ – the first and the second initial compositions respectively; ◆,▲,● – ternary eutectic points according to SEM/EDX analysis for the first test, the second test, and the average value respectively; the binary eutectic compositions provided by corresponding references: ■ – [5,6]; ◥ – [9,10].

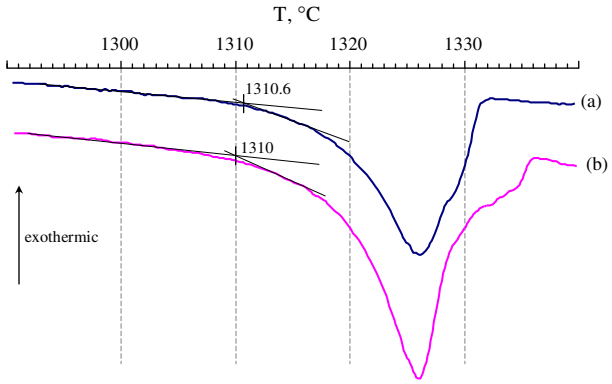

Fig. 7. DTA curves of the samples cut out from the ingot eutectic zone: (a) – SQ5 region (Fig. 2, Table 1), (b) – SQ1 region (Fig. 3, Table 1).

which overestimates the solidus temperature Galakhov [25] in comparison with DTA, by contrast, the latter underestimates the onset melting temperature due to eutectic interaction of a sample with the crucible material (Al_2O_3) Bechta et al. [6,10]. For this reason we consider the thermal effects following the eutectic one, as related to liquidus of the FeO_{1+x}–UO_2–ZrO_2–Al_2O_3 system.

The data obtained were used for the construction of the FeO_{1+x}-enriched region in a 3D FeO_{1+x}–UO_2–ZrO_2 phase diagram (Fig. 8). It is noted that the low temperature eutectic zone for this system is already relatively limited. The area for the solidus temperature minimum is a narrow 'trough' that lies between 96.0 FeO_{1+x}–4.0 UO_2 (mol.%), the ternary eutectic and the 89.8 FeO_{1+x}–10.2 ZrO_2 (mol.%)[2] compositions (two binary eutectic points and the ternary eutectic point marked by a line in Fig. 8). However, for higher ZrO_2 and UO_2 contents the liquidus surface rises rapidly and lies below the FeO_{1+x} melting in the 1371–1379 °C temperature range compared to Darken and Gurry [7] and Wriedt [28] only for the FeO_{1+x}-rich zone within the 93.5 FeO_{1+x}–6.5 UO_2, 91.5 FeO_{1+x}–4.5 UO_2–5.0 ZrO_2, 89.0 FeO_{1+x}–11.0 ZrO_2 (mol.%) boundary. This information is useful for prediction of phase fusion/solidification under severe accident conditions, in particular during core melt in-vessel retention as well as for the optimization of the European Thermodynamic Database for Corium Cheynet [20], i.e. the non ideal NUCLEA database as in Bakardjieva et al. [23]. A first comparison between NUCLEA and the obtained experimental data in the present experimental study has been performed. The calculated liquidus temperature for the composition 91.8 $Fe_{0.947}O$–3.8 UO_2–4.4 ZrO_2 (mol.%) is predicted to be 1318 °C, i.e. in very good agreement with the experimental determination (1310 °C) corresponding to the eutectic composition. The slight difference could be solved by an experimental investigation of the UO_2–Fe_2O_3 phase diagram which remains, today, uncertain (Petrov et al. [29]).

[2] In the ZrO_2–FeO_{1+x} phase diagram it should be a two phase region in the very narrow temperature range (1371–1379 °C) as it is in Fig. 8 and in the UO_2–FeO_{1+x} diagram (Fig. 1a) and Bechta [6]) although nature of the melting of FeO_{1+x} phase this was not pointed out in our previous publication (Bechta [10]).

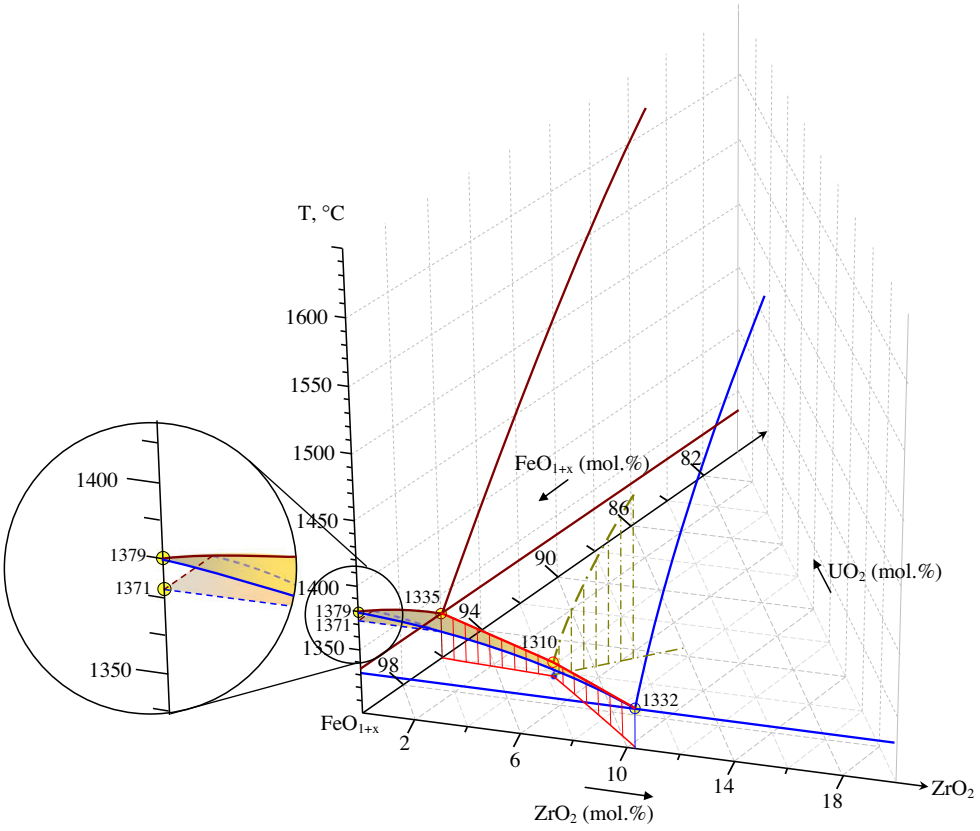

Fig. 8. 3D Phase diagram of the FeO_{1+x}–UO_2–ZrO_2 system in the FeO_{1+x}-rich region (neutral atmosphere).

4. Conclusions

The eutectic temperature of 1310–1315 °C and ternary eutectic composition of 91.8 ± 0.5–FeO_{1+x}–3.8 ± 0.3 UO_2–4.4 ± 0.4 ZrO_2 (mol.%) in the FeO_{1+x}–UO_2–ZrO_2 system have been determined in a neutral atmosphere. The composition of the UO_2(ZrO_2, FeO_{1+x}) solid solution has been determined as 79.2 ± 1.2 UO_2–10.8 ± 1.9 ZrO_2–10.0 ± 1.6 FeO_{1+x} (mol.%) at the eutectic temperature. A 3D phase diagram of the FeO_{1+x}–UO_2–ZrO_2 system in the FeO_{1+x}-rich region has been constructed, which shows that the liquidus temperature is below that of pure FeO_{1+x} only for additions of ZrO_2 + UO_2 to FeO_{1+x} between 6.5 and 11 mol.%.

The measured composition of the ZrO_2-rich phase appears to be too low in Zr when compared with extrapolations based on the ZrO_2–UO_2 phase diagram and will require further analysis to confirm the position of the FeO_{1+x}–ZrO_2 boundary tie-line.

Acknowledgements

This work was supported by the ISTC (Project #1950.2). The authors express their gratitude to Dr. M. Hugon (EU), Dr. V.Ya. Rudneva (ISTC) and Dr. Yu.N. Aniskevich (NITI) for the research coordination, the engineers A.V. Lysenko, V.R. Bulygin, R.A. Kosarevsky and Dr. S.Yu. Kotova (NITI) for their activity in the IMCC and DTA experimental work, M.D. Tolkachev[1] (IPGG RAS) for SEM/EDX analysis.

References

[1] H. Tuomisto, T.G. Theofanous, Nucl. Eng. Des. 148 (1994) 171.
[2] S.V. Bechta, V.B. Khabensky, S.A. Vitol, E.V. Krushinov, V.S. Granovsky, D.B. Lopukh, V.V. Gusarov, A.P. Martinov, V.V. Martinov, G. Fieg, W. Tromm, D. Bottomley, H. Tuomisto, Nucl. Eng. Des. 236 (2006) (1362 and 1810).
[3] B. Adroguer, Corium interactions and thermochemistry in EU co-sponsored research on reactor safety, severe accidents, in: A. Zurita, G. Van Goethem (Eds.), Final Summary Reports – 'INV' Cluster Projects, EC Project Report EUR 19960 EN, 2003.
[4] D. Lopukh, S. Bechta, A. Pechenkov, S. Vitol, K. Froment, S. Hellmann, M. Fischer, B. Duret, J.M. Seiler, in: Proceedings of the ICONE 8 of 8th International Conference on Nuclear Engineering, Baltimore, Maryland, USA, 2–6 April, 2000 (ICONE-8179).
[5] S.V. Bechta, E.V. Krushinov, V.I. Al'mjashev, S.A. Vitol, L.P. Mezentseva, Yu.B. Petrov, D.B. Lopukh, N.A. Lomanova, V.B. Khabensky, M. Barrachin, S. Hellmann, K. Froment, M. Fischer, W. Tromm, D. Bottomley, V.V. Gusarov, Radiochemistry 49 (2007) 20.
[6] S.V. Bechta, E.V. Krushinov, V.I. Almjashev, S.A. Vitol, L.P. Mezentseva, Yu.B. Petrov, D.B. Lopukh, V.B. Khabensky, M. Barrachin, S. Hellmann, K. Froment, M. Fisher, W. Tromm, D. Bottomley, V.V. Gusarov, J. Nucl. Mater. 362 (2007) 46.
[7] L.S. Darken, R.W. Gurry, J. Am. Chem. Soc. 67 (1945) 1398.
[8] W.A. Fischer, A. Hoffmann, Archiv für das Eisenhüttenwesen 28 (1957) 739.
[9] S.V. Bechta, E.V. Krushinov, V.I. Almjashev, S.A. Vitol, L.P. Mezentseva, Yu.B. Petrov, D.B. Lopukh, V.B. Khabensky, M. Barrachin, S. Hellmann, V.V. Gusarov, Russ. J. Inorg. Chem. 51 (2006) 325.
[10] S.V. Bechta, E.V. Krushinov, V.I. Almjashev, S.A. Vitol, L.P. Mezentseva, Yu.B. Petrov, D.B. Lopukh, V.B. Khabensky, M. Barrachin, S. Hellmann, K. Froment, M. Fisher, W. Tromm, D. Bottomley, F. Defoort, V.V. Gusarov, J. Nucl. Mater. 348 (2006) 114.
[11] W.A. Lambertson, M.H. Mueller, J. Am. Ceram. Soc. 36 (1953) 365.
[12] G.M. Wollten, J. Am. Chem. Soc. 80 (1958) 4772.
[13] P.E. Evans, J. Am. Ceram. Soc. 43 (1960) 443.
[14] N.M. Voronov, E.A. Voytekhova, I.T. Kovalev, in: Structures of Alloys in Some Systems Containing Uranium and Thorium (Transactions of the A.A. Baykov Institute of Metallurgy RAS), Moscow, Gosatomizdat, 1961, pp. 467–481 (in Russian).
[15] N.M. Voronov, R.M. Sofronova, E.A. Voytekhova, High-Temperature Chemistry of Uranium Oxides and their Compounds, vol. 358, Atomizdat, Moscow, 1971 (in Russian).
[16] J. Cohen, B.E. Schaner, J. Nucl. Mater. 9 (1963) 18.
[17] C.F. Baes, J.H. Shaffer, H.F. McDuffie, Trans. Am. Nucl. Soc. 6 (1963) 393.
[18] P.D. Bottomley, M. Coquerelle, Nucl. Technol. 87 (1989) 120.
[19] A. Skokan, FZK Technical Report, KFK 3880/2, December 1984.
[20] B. Cheynet, NUCLEA, Nuclear Thermodynamic Database, THERMODATA, 2007. <http://hal.archives-ouvertes.fr/hal-00165418/>.
[21] P.Y. Chevalier, E. Fischer, B. Cheynet, CALPHAD 28 (2004) 15.
[22] K.A. Romberger, C.F. Baes, H.H. Stone, J. Inorg. Nucl. Chem. 29 (1967) 1619.

[23] S. Bakardjieva, M. Barrachin, S. Bechta, D. Bottomley, L. Brissoneau, B. Cheynet, E. Fischer, C. Journeau, M. Kiselova, L. Mezentseva, P. Piluso, T. Wiss, Prog. Nucl. Energy 52 (2010) 84.
[24] Yu.B. Petrov, Induction Melting of Oxides, Energatomizdat Publishers, Leningrad, Leningrad Branch, 1983 (in Russian).
[25] F.Ya. Galakhov, Zavodskaya Laboratoria 17 (1951) 254 (in Russian).
[26] V.I. Almjashev, V.V. Gusarov, O.V. Mazurin, New achievement in chemistry and material technology, in: Proceedings of the Conference, Saint-Petersburg, 2002, p. 62.
[27] N.A. Toropov, V.P. Barzakovsky, I.A. Bondar et al., Constitution Diagrams of Silicate Systems, Handbook, Issue 2, Metal-Oxygen Compounds of Silicate Systems, Nauka Publishers, Leningrad, 1969 (in Russian).
[28] H.A. Wriedt, J. Phase Equil. 12 (1991) 170.
[29] Y.B. Petrov, Y.P. Udalov, J. Subrt, S. Bakardjieva, P. Sazavsky, M. Kiselova, P. Selucky, P. Bezdicka, C. Journeau, P. Piluso, Glass Physics and Chemistry 35 (3) (2009) 296.